Journal of Geophysical Research: Solid Earth

Supporting Information for

Constraints on the depth, thickness, and strength of the G discontinuity in the central Pacific from S receiver functions

H. F. Mark[1], J. A. Collins[2], D. Lizarralde[2], G. Hirth[3], J. B. Gaherty[4], R. L. Evans[2], and M. D. Behn[5]

[1]Department of Earth and Planetary Sciences, Washington University in St. Louis, [2]Department of Geology and Geophysics, Woods Hole Oceanographic Institution, [3]Geological Sciences Department, Brown University, [4]School of Earth and Sustainability, Northern Arizona University, [5]Department of Earth and Environmental Sciences, Boston College

Contents of this file

Additional Supporting Information (Files uploaded separately)

Text S1.

A variety of methods can be used to generate synthetic seismograms for synthetic receiver function calculations, and reflectivity synthetics are more complex and computationally expensive than some commonly used ray theory-based methods. Here, we briefly discuss the costs and benefits of reflectivity synthetics, and in particular highlight the utility of the reflectivity method for calculating realistic delay times between direct and converted seismic phases.

Reflectivity synthetics account for the full response of a layered velocity model to a seismic source (Kennett & Kerry, 1979). This means that a seismogram calculated for a particular source-station range will automatically include reflected and converted phases, and each phase that arrives corresponds to the appropriate ray parameter for that phase at that range. Reflectivity synthetic seismograms are thus an accurate representation of the wavefield recorded at a given range, provided the velocity model used for the calculation is accurate. This accuracy comes at some computational expense, as numerical integration of the wavefield requires the calculation of the model response over densely spaced frequencies and ray parameters in order to avoid aliasing.

Synthetic seismograms calculated with ray-based methods are much faster. Commonly used codes such as *Raysum* (Frederiksen & Bostock, 2000) use ray-theoretical traveltimes to construct a synthetic seismogram for a range, a set of phases, and a single ray parameter specified by the user. This is reasonable for sets of phases with very similar ray parameters, but it does require the user to pick an appropriate ray parameter for a given range, and the phase arrival times will not all perfectly correspond to the range since, in reality, different phases recorded at one station will have different ray parameters.

Synthetic receiver functions illustrate how different methods of calculating seismograms result in different levels of complexity that propagate through to the receiver function calculation (Figure S1). Synthetics based on *Raysum* result in receiver functions with a simple shape; this is expected since the phases included in the seismogram are limited to direct *S* and *S*-to-*p* conversions at G and the Moho (Figure S1a). More complex synthetics can be generated with this code, but all phases have to be explicitly specified. The results of the *Raysum* calculation can be compared to a similar, though not identical, calculation where receiver functions are obtained from a τ trace at a single p; this is effectively a reflectivity calculation before the integration step where synthetics are transformed to the T-X domain, so the trace does not technically correspond to a single range. The receiver function stack from this trace has a more complex shape than the *Raysum* version, since the trace used for the calculation automatically includes any and all reflections and conversions in the velocity model (Figure S1b). Both the *Raysum* and the τ-p receiver functions have clear peaks corresponding to the G conversion, at the time predicted for the converted phase arrival for the specified p.

Receiver functions calculated using full reflectivity synthetics have a more complex shape, but still have a negative lobe around the time that ray theory predicts for a G conversion to arrive (Figures S1c, d). These synthetics do not require us to choose a ray parameter a priori, but rather include all direct, converted, and reflected phases at appropriate ray parameters for the specified range. Thus, when we pick the time of the negative peak corresponding to the G conversion from these receiver function stacks, we can avoid embedding assumptions about ray parameters and automatically include the effects of any interfering phases without explicitly specifying what those phases might be.

A more detailed discussion of the effects of using a single ray parameter vs many ray parameters in synthetic seismograms can be found in Marson-Pidgeon and Kennett (2000).

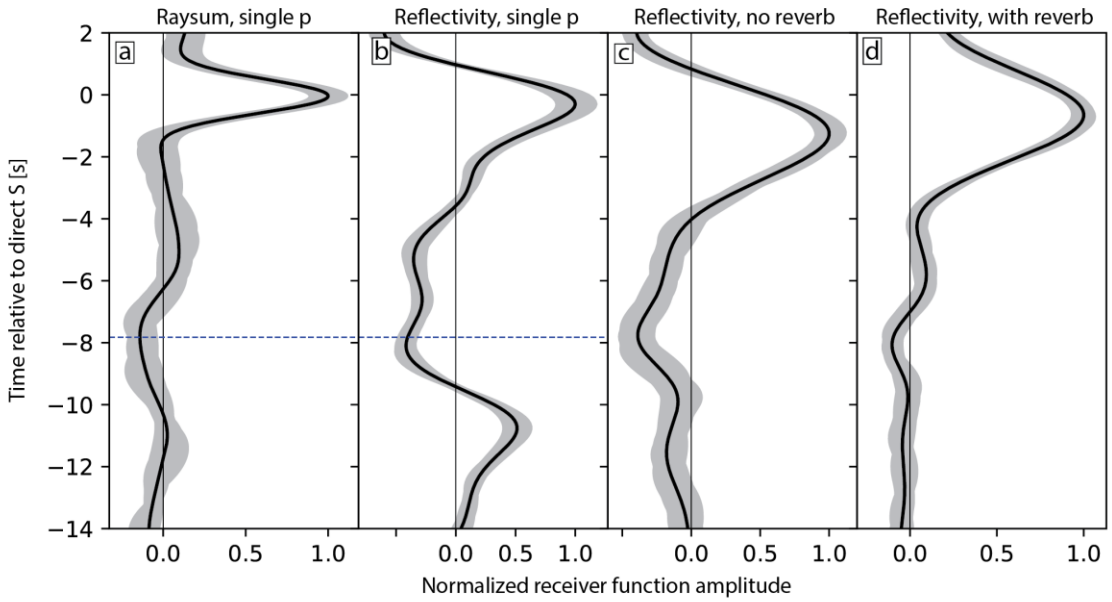

Figure S1. Comparison of synthetic receiver functions calculated with ray theoretical and reflectivity codes. All sets of synthetic seismograms were calculated using a 1D velocity model where a G discontinuity is imposed at 70 ± 0 km depth with a strength of 7.5%. The seismograms for (a), (c), and (d) were calculated for a source-station distance of 70º. Noise sampled from the NoMelt data was added to each synthetic seismogram before calculating the receiver functions. The addition of many different noise samples is used to obtain an ensemble of receiver functions based on each single seismogram. Solid lines show the stack of all receiver functions, and grey shading shows the full range of values obtained from the bootstrap stacks. Bootstrap stacking methods are described in Section 2.3 of the main text. The dashed blue line in (a) and (b) shows the calculated arrival time of the *S*-to-*p* conversion at G for that particular ray parameter. **(a)** Synthetic receiver functions calculated using seismograms from the ray theoretical code *Raysum* using a ray parameter of 0.08 (Frederiksen & Bostock, 2000). The *Raysum* seismograms only include converted phases from the Moho and the G discontinuity. **(b)** Synthetic receiver functions calculated from a single τ-p trace obtained using a version of B. L. N. Kennett's reflectivity code (Kennett & Kerry, 1979). The p for this trace is 0.08, as in (a). **(c)** Reflectivity synthetic receiver functions calculated using full synthetics, integrated for a 70º range. Reverberations within layers of the velocity model are not included. **(d)** Reflectivity synthetic receiver functions calculated using full synthetics similar to (c). Reverberations within all layers of the velocity model are included.

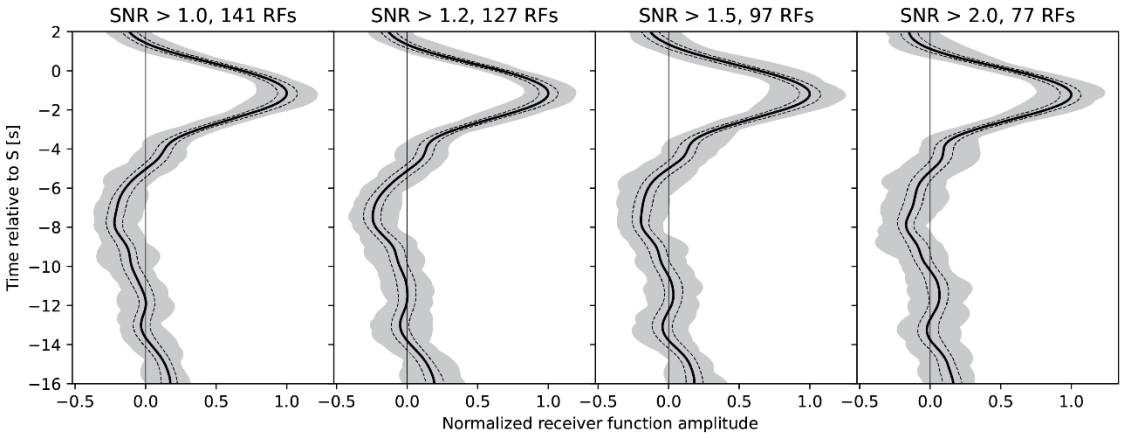

Figure S2. Synthetic receiver function stacks made using different signal-to-noise ratio (SNR) thresholds. The synthetics correspond to a model with G at 60 ± 2.5 km depth and a Vsv drop of 10.5%. Noise sampled from the data is added to the synthetic seismograms before the receiver function calculations, and the SNR is calculated from the data as described in the main text (Section 2.2). Raising the minimum SNR threshold reduces the number of traces available for stacking.

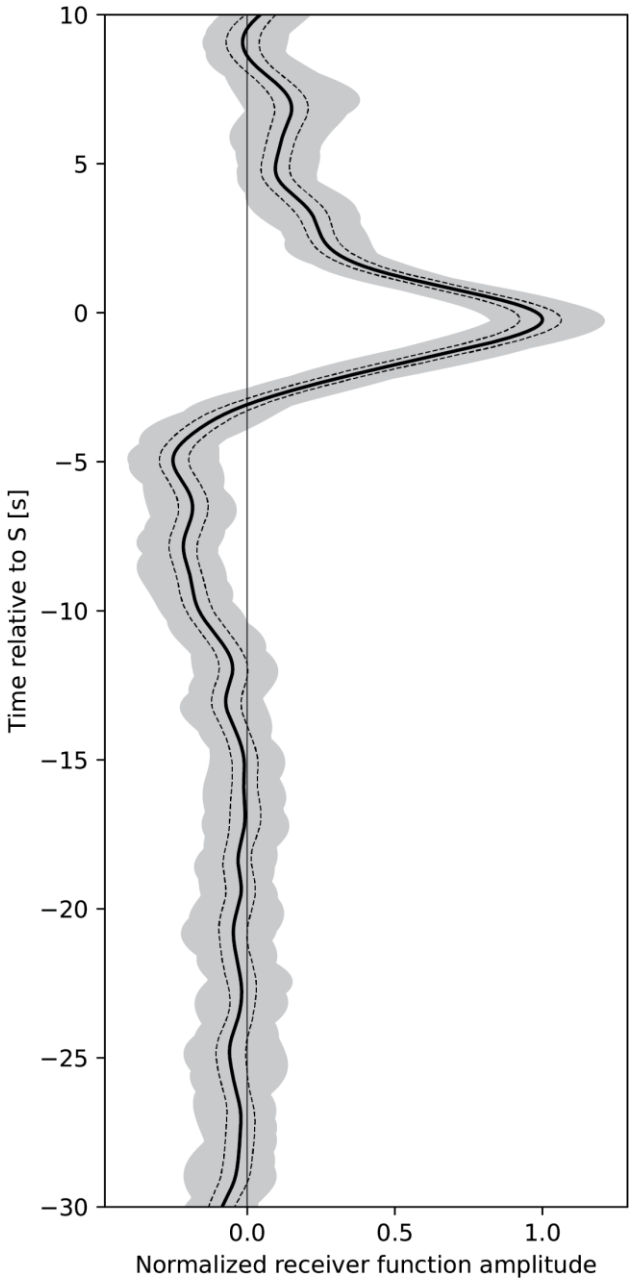

Figure S3. The observed receiver function stack, with moveout corrections calculated using a velocity model with G at 65 ± 0 km as a 7.5% drop in Vsv. The solid black line is the overall stack of 125 receiver functions. Dashed black lines show one standard deviation of amplitudes from bootstrap stacks, and grey shading shows the full range of amplitudes from bootstrap stacks. Bootstrap stacking methods are described in Section 2.3 of the main text. Besides the Moho side lobe at approximately -5 seconds and the peak we attribute to the G conversion at approximately -8 seconds, the receiver function stack does not show any significant negative or positive peaks in the window 30 seconds prior to direct *S*.

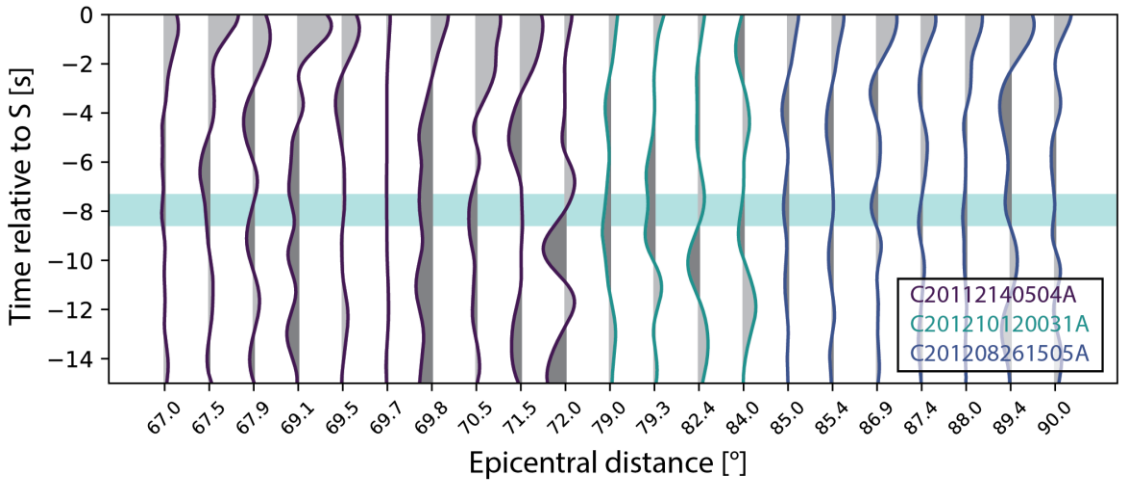

Figure S4. Individual, unstacked receiver functions from three events. These receiver functions are corrected for moveout using a model with a 7.5% step-function drop in Vsv at 65 km depth, and are normalized by the maximum amplitude across all the traces shown in the figure. The traces are ordered by epicentral distance but plotted with even spacing along the horizontal axis for ease of viewing. Traces are color-coded by event, with event IDs provided in the legend. The shaded light blue band shows the range of peak times obtained from the receiver function stacks.

Supporting References

Frederiksen, A. W., & Bostock, M. G. (2000). Modelling teleseismic waves in dipping anisotropic structures. *Geophysical Journal International*, *141*(2), 401–412.

Kennett, B. L. N., & Kerry, N. J. (1979). Seismic waves in a stratified half space. *Geophysical Journal International*, *57*(3), 557–583. https://doi.org/10.1111/j.1365-246X.1979.tb06779.x

Marson-Pidgeon, K., & Kennett, B. L. N. (2000). Flexible computation of teleseismic synthetics for source and structural studies. *Geophysical Journal International*, *143*(3), 689–699. https://doi.org/10.1046/j.1365-246X.2000.00268.x

Table S1. Event-station pairs used in this study. The columns are CMT event name and station name. Filename: 2019JB019256-table01.dat

Table S2. Models that are found to be consistent with the observed receiver functions. The file contains 10 models, in no particular order. For each model, a model name is given, followed by column headers and columns of model parameters: Depth (km), Vpv (km/s), Vsv (km/s), density (g/cc), Qp, and Qmu. Filename: 2019JB019256-table02.dat